ISSN 0208-7774 T R I B O L O G I A 4/2021 p. 45–55
DOI: 10.5604/01.3001.0015.8368

Mirosław SZALA*

CAVITATION EROSION PHENOMENOLOGICAL MODEL OF MCrAlY AND NiCrMoNbTa METALLIC COATINGS DEPOSITED VIA THE HVOF METHOD

FENOMENOLOGICZNY MODEL EROZJI KAWITACYJNEJ METALOWYCH POWŁOK MCrAlY I NiCrMoNbTa NATRYSKIWANYCH METODĄ HVOF

Key words: cavitation erosion, failure analysis, wear mechanism, thermal spraying, microstructure, roughness, erosion rate.

Abstract: The work describes the phenomenological model of cavitation erosion (CE) elaborated for MCrAlY (where M = Co, Ni or Co/Ni) and NiCrMoNbTa. Coatings were deposited via the HVOF method from CoNiCrAlY, NiCoCrAlY and NiCrMoNbTa feedstock powders. CE tests, conducted according to ASTM G32 standard, indicate that MCrAlYs have a 50% higher maximum erosion rate and twice lower CE resistance than the NiCrMoNbTa coating. CE kinetics of coatings were comparatively studied, combining the mass loss, erosion rate, roughness changes of the eroded surface with microstructure, and mechanical properties of the coatings. Results of SEM analysis of damaged coatings allow identifying the mechanism of CE. In the case of both types of coatings, the erosive damage is initiated at the removal of loose splats, cracking at the border splats and peeling off the coating material, and surface pitting. However, NiCrMoNbTa, due to higher ductility and microstructure homogeneity, presents lesser surface pitting contrary to the MCrAlYs, which have multiphase microstructure higher hardness and consequently was prone to cracking, resulting in the formation of craters and higher surface roughening. The CE mechanism of MCrAlYs was dominated by the brittle mode, while the NiCrMoNbTa coating has mainly a ductile damage behaviour.

Słowa kluczowe: erozja kawitacyjna, analiza uszkodzeń, mechanizm zużycia, natryskiwanie termiczne, mikrostruktura, chropowatość, szybkość erozji.

Streszczenie: W pracy opisano fenomenologiczny model erozji kawitacyjnej (EK) opracowany dla powłok MCrAlY (gdzie M = Co, Ni lub Co/Ni) i NiCrMoNbTa. Powłoki wytworzono metodą HVOF z komercyjnych proszków CoNiCrAlY, NiCoCrAlY i NiCrMoNbTa. Testy erozji kawitacyjnej, przeprowadzone zgodnie z normą ASTM G32, wskazują, że MCrAlY mają o 50% wyższą prędkość erozji i dwukrotnie niższą odporność EK niż powłoka NiCrMoNbTa. Kinetyka erozji kawitacyjnej powłok została poddana analizie porównawczej syntetyzującej utratę masy, szybkość erozji, zmiany chropowatości erodowanej powierzchni z mikrostrukturą oraz właściwościami mechanicznymi badanych powłok. Wyniki analizy SEM uszkodzonych powłok umożliwiły zidentyfikowanie mechanizmu EK. Uszkodzenie erozyjne powłok inicjowane jest w wyniku usuwaniu słabo umocowany cząstek materiału, pękaniu na granicach lameli następnie usuwaniu materiału i tworzeniu wżerów. Jednak NiCrMoNbTa ze względu na wyższą ciągliwość i jednorodność mikrostruktury wykazuje mniejsze wżery powierzchniowe w przeciwieństwie do MCrAlYs, które cechują się wielofazową mikrostruktura o wyższej twardości i w konsekwencji są podatne na pękanie, co powoduje powstawanie dużych wżerów i wyższe chropowacenie powierzchni. Mechanizm erozji kawitacyjnej powłok MCrAlY jest zdominowana przez kruche pękanie, natomiast w przypadku powłoki NiCrMoNbTa dominuje plastyczne odkształcenie.

* ORCID: 0000-0003-1059-8854. Lublin University of Technology, Faculty of Mechanical Engineering, Department of Materials Engineering, Nadbystrzycka 36D Street, 20-618 Lublin, Poland.

INTRODUCTION

The thermal spraying process meets its application in many types of industries. For example, it is used in the aerospace industry, automotive engineering, as well as in maritime sectors. One of the most popular thermal spraying methods is the HVOF (high velocity oxygen-fuel). The HVOF method is widely applied in anti-wear solutions, mainly due to the fact that it retains lower oxidation and decomposition of deposited material, and has a dense microstructure and low porosity and high adhesion to the substrate, especially in comparison to other thermal spray techniques **[L. 1–4]**. Among others, a promising application of the HVOF method is preventing of metallic substrate from cavitation erosion **[L. 5–7]**.

Cavitation erosion (CE) is a material degradation process due to harmful fluid action initiated by pressure fluctuations in the liquid. When the liquid pressure drops, the vapour can grow, and as the pressure increases, the vapour bubbles implode. The resulting emission of shock waves and liquid-jet cause degradation of a solid material **[L. 8]**. CE can deteriorate the service life of machinery and equipment **[L. 9–11]**. HVOF methods enable the deposition of a wide range of engineering materials, including metals, cermets, or ceramic-based coatings. Generally, the HVOF coatings constituted of nickel or/and cobalt-based powders are very often used as a protective layer **[L. 12–14]**. Although, in terms of cavitation erosion, it is believed that cobalt-based materials present one of the highest cavitation erosion resistances **[L. 15–18]**. On the other hand, the nickel-based materials also give interesting anti-cavitation erosion results **[L. 19–21]**.

CE mechanisms investigations are essential for understanding the factors influencing the CE resistance of nickel-cobalt containing materials. Unfortunately, literature regarding HVOF metallic coatings gives scant information about it. Available data mainly describes models of cavitation erosion for different types of coatings and deposition methods exemplary flame-sprayed Al_2O_3-40%TiO_2/NiMoAl composite coatings **[L. 22]**, modified APS-ceramic/organic coatings **[L. 23]**, HVOF sprayed WC–12Co **[L. 24]**, WC-10Co4Cr **[L. 25]**, Ni-Cr-Al_2O_3 **[L. 26]** and NiCoCrAlYTa **[L. 27]** coatings. However, the literature survey indicates that cermets and composite HVOF coatings CE damage models dominate. Phenomenological models of cavitation erosion of metallic HVOF coatings MCrAlY (where M = Co, Ni or Co/Ni) and NiMoCrNbTa are scant. Moreover, there is still a lack of relevant research presenting a model combining the microstructure features and hardness with surface morphology changes due to cavitation. This attempt is useful to clarify the kinetics of cavitation erosion. From both scientific and technological points of view, it seems interesting to visualize the cavitation erosion process of HVOF metallic coatings. Results broaden the state's knowledge about the phenomena during the CE process of nickel and cobalt-based coatings and clarify the properties of HVOF metallic coatings promoting their anti-cavitation behaviour.

This work elaborates on the CE phenomenological model of the HVOF deposited MCrAlY and NiCrMoNbTa coatings. This model combines coatings properties with cavitation erosion material loss and changes of damaged surface roughness.

MATERIALS AND METHODS

Coatings characterization

The paper continues the research initiated in a previous paper for HVOF coatings deposited on Inconel 617 substrate **[L. 28]**. The study reveals the phenomenological CE model of thermally sprayed metallic coatings. Coatings were thermally sprayed via the HVOF method using MCrAlY and NiCrMoNbTa commercial powders, see **Tab. 1**. Typical applications of MCrAlY are bond coat for TBC ceramics, protection against oxidation and high-temperature corrosion and, in the case of NiCrMoNbTa, coating surface regeneration of nickel-based components. It is worth investigating the CE resistance of those coatings mainly because the professional literature describes cobalt and nickel-based materials as highly resistant to CE damage. Thus, coatings chemical composition (Ni and Co content) and hardness differ, see **Tab. 1**. The mean hardness of the investigated coatings ranges from 341HV0.1 to 393HV0.1. Metallographic and phase composition studies, done in previous work **[L. 28]**, confirm that the microstructure of A and C coatings is dominated by a single-phase solid solution microstructure, while B coating presents a two-phase microstructure. In addition, all coatings present typical for HVOF as-sprayed coatings lamellar microstructure. These are important factors affecting CE behaviour.

Table 1. Specimens codes, coatings hardness and characterization of feedstock powders used for HVOF spraying, on the basis of [L. 28]

Tabela 1. Oznaczenia próbek, twardość powłok oraz charakterystyka proszków użytych do natryskiwania metodą HVOF, na podstawie **[L. 28]**

Specimen code	**A**	**B**	**C**
Alternate name	CoNiCrAlY	NiCoCrAlY	NiCrMoNbTa
Feedstock grade	Amdry 9954	Ni-191-4	Diamalloy 1005
Hardness, HV0.1	365±28	393±27	341±37
Chemical composition of feedstock powder, wt%			
Ni	29.0–35.0	Bal.	Bal.
Co	Bal.	22.0	–
Cr	18.0–24.0	17.0	21.5
Al	5.0–11.0	12.5	–
Y	0.1–0.8	0.55	–
Mo	–	–	9.0
Nb+Ta	–	–	3.7
Fe	–	–	2.5

Cavitation erosion testing

The cavitation erosion resistance tests were carried out in accordance with the ASTM G32 standard **[L. 29]**. The sonotrode tip distance from the sample was 1mm ± 0.05 mm, the medium in which cavitation was induced was distilled water, see **Fig. 1**. The analysis of the resistance to cavitation erosion consisted of systematic measurements of the weight loss of the tested samples with an accuracy of 0.01 mg. In the current study, the total exposure time lasted 3 hours. To obtain reliable erosive results, the test surfaces were uniformly treated. The as-sprayed coatings were finished by grinding and roughness equals Ra < 5.28 μm, Rt < 38.3 μm Rz < 28.5 μm and RSm < 0.125 mm. The cavitation erosion mechanisms of the eroded surfaces were examined at stated time intervals of the cavitation testing. The surface roughness Ra, Rt, Rz, RSm parameters were determined using the surface profiler (Surtronic S-128, Taylor-Hobson, Leicester, UK) according to the ISO 4287 standard. Eroded surfaces roughness parameters were measured in profiles obtained in two perpendicular directions. Finally, SEM (Scanning Electron Microscopy) analyses of damaged surfaces and coatings cross-sections were carried out. Combining the properties of the coatings with the observation of cavitation damaged surfaces allows the elaboration of the phenomenological model of CE of HVOF metallic coatings.

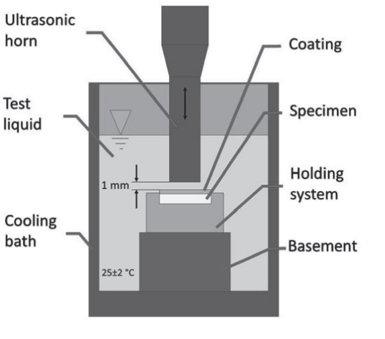

Fig. 1. Schematic representation of the ultrasonic vibratory system used for cavitation

Rys. 1. Schemat urządzenia ultradźwiękowego użytego w badaniach kawitacyjnych

RESULTS AND DISCUSSION

Characterization of the cavitation erosion (CE) results

Cavitation erosion mass loss and erosion rate curves are presented in **Figs. 2, 3** shows changes in the roughness versus exposure time. It was revealed in a previous study that **[L. 28]** the coatings present increasing resistance to cavitation erosion in the following order: NiCoCrAlY < CoNiCrAlY < NiCrMoNbTa. As a result, MCrAlYs have the highest material losses, contrary to NiCrMoNbTa, which present 50% lower mean depth of erosion (MDE), **Fig. 2a** and the lowest erosion rate (ER),

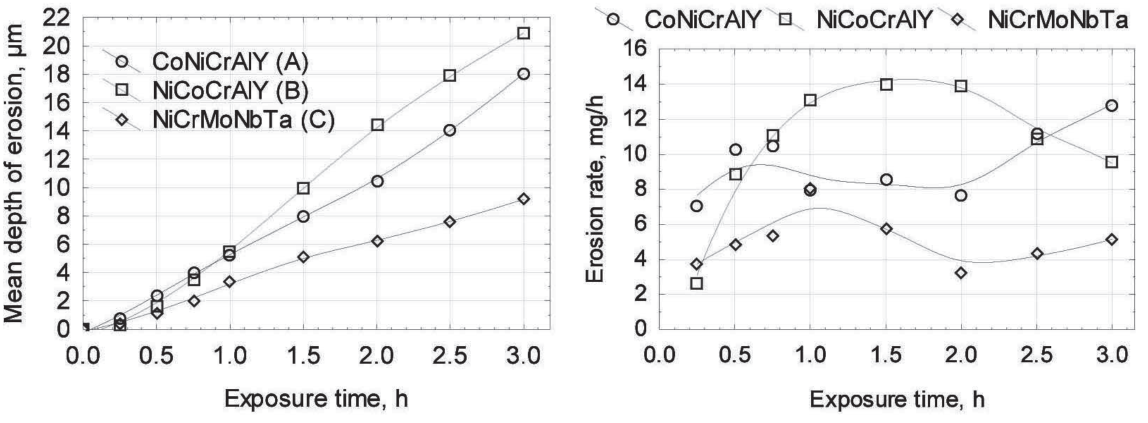

Fig. 2. Cavitation erosion curves: mean depth of the erosion (MDE) (a) and erosion rate (ER) (b) (based on results given in [L. 28])

Rys. 2. Krzywe kawitacyjne: (a) średnia głębokość erozji (MDE) oraz (b) prędkość erozji (ER); na podstawie rezultatów przedstawionych w [**L. 28**])

Fig. 2b. Generally, MCrAlYs coatings have comparable maximal erosion rates, 50% exceeding those reported for NiCrMoNbTa (C) coatings (8 mg/h). Besides, the NiCoCrAlY (B) coating obtained a maximal erosion rate at earlier stages than in the case of CoNiCrAlY (A).

Surface roughness absolute parameters, likewise Rz, Ra, Rt or RSm, increase with exposure time, **Fig. 3**; although, the analysis of each specific roughness parameter indicates that changes do not proceed linearly vs exposure time. The highest goodness of fit was recognized for MDE and Rz parameters see **Fig. 4** and **Tab. 2**. Overall, it seems that specific absolute parameters alone, like Ra, Rt etc, do not fully correlate with the erosion depth (MDE), (see **Tab. 2**); however, it provides essential information about the depth (Rz, Rt), with (RSm) and uniformity (Ra) of eroded surface. Therefore, an originally proposed factor – roughness rate, RR for the overall roughness characterization of cavitation eroded surfaces was proposed, see Equation (1) and **Fig. 3d**. RR factor combines the width (RSm), high (Rt) of roughness profile, and mean roughness (Ra) parameters vs. specific exposure time (t).

$$\mathrm{RR}(\mathrm{t}) = \frac{RSm(t) \cdot \left[Ra(t) - Ra_{t0} \right]}{Rt(t)}, \mu m \qquad (1)$$

RR gives information about CE surface damage and also relates to the kinetics of CE process. It was shown by the literature that CE material loss of metal alloys does not proceed linearly with exposure time **[L. 9, 17]**. Besides, the response of the thermally sprayed coatings to CE loads is even much more complex. The simultaneous processes took place during CE of HVOF coatings likewise, non-steady material removal and the growth of randomly located pits, the appearance of craters, fatigue, cracking, plastic deformation, and material detachment, visualized in SEM photos **Fig. 5a–c**. On the other hand, analysis of specific roughness parameters fulfil information about the cavitation erosion damage at a specific time interval, i.e. well characterizes the depth, width or surface morphology uniformity of eroded coatings vs. time. Roughness analysis enables the understanding of CE kinetics, the CE damage mechanism, and facilitates elaborating the CE phenomenological model of HVOF coatings, **Fig. 6**.

Table 2. Coefficients of determination (r^2) estimated for mean erosion depth of erosion, MDE (independent variable) and roughness parameters (dependent variable)

Tabela 2. Współczynniki determinacji (r^2) wyznaczone dla średniej głębokości erozji, MDE (zmienna niezależna) oraz parametrów chropowatości (zmienna zależna)

Coating type / Roughness	Coefficient of determination, r^2		
	A	B	C
Rz	0.895	0.889	0.725
Rt	0.840	0.713	0.608
Ra	0.791	0.875	0.373
RSm	0.850	0.638	0.335
Rz/Ra	0.688	0.044	0.721
RR factor	0.574	0.783	0.177

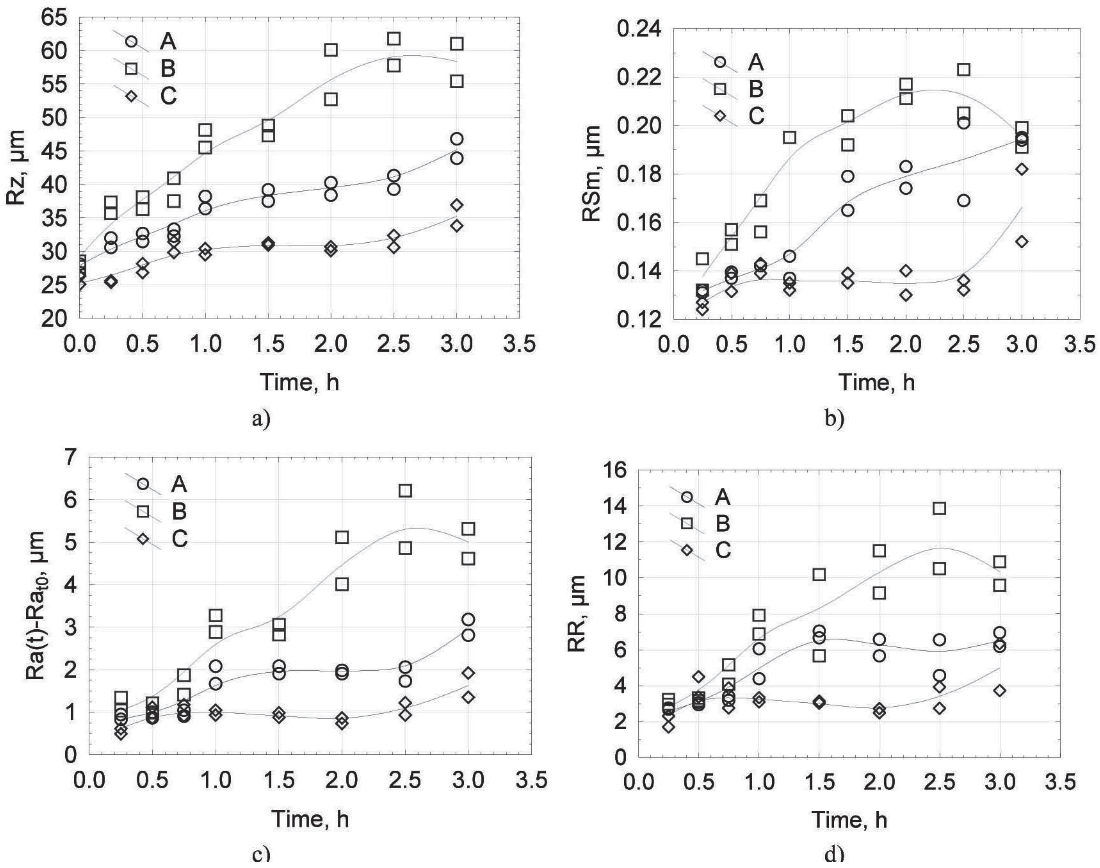

Fig. 3. Fluctuations of roughness parameters vs exposure time (t). Absolute values of: a) Rz, b) RSm, c) increase rate of Ra roughness, d) Roughness rate (RR) factor

Rys. 3. Zmiana parametrów chropowatości względem czasu ekspozycji na kawitację (t). Parametry bezwzględne: a) Rz, b) RSm, c) zmiana wartości parametru Ra, d) współczynnik zmiany chropowatości (RR)

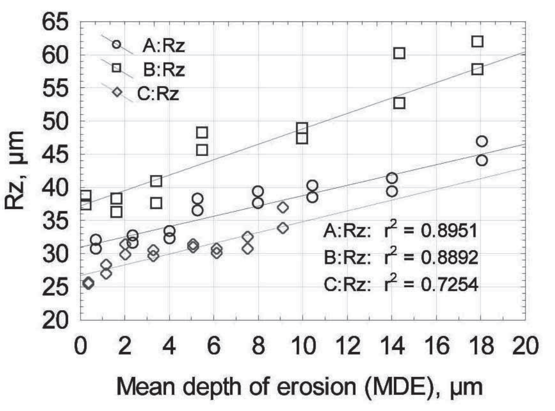

Fig. 4. Correlation between the mean erosion depth (MDE) and Rz roughness parameter

Rys. 4. Zależność pomiędzy średnią głębokością erozji (MDE) oraz parametrem chropowatości Rz

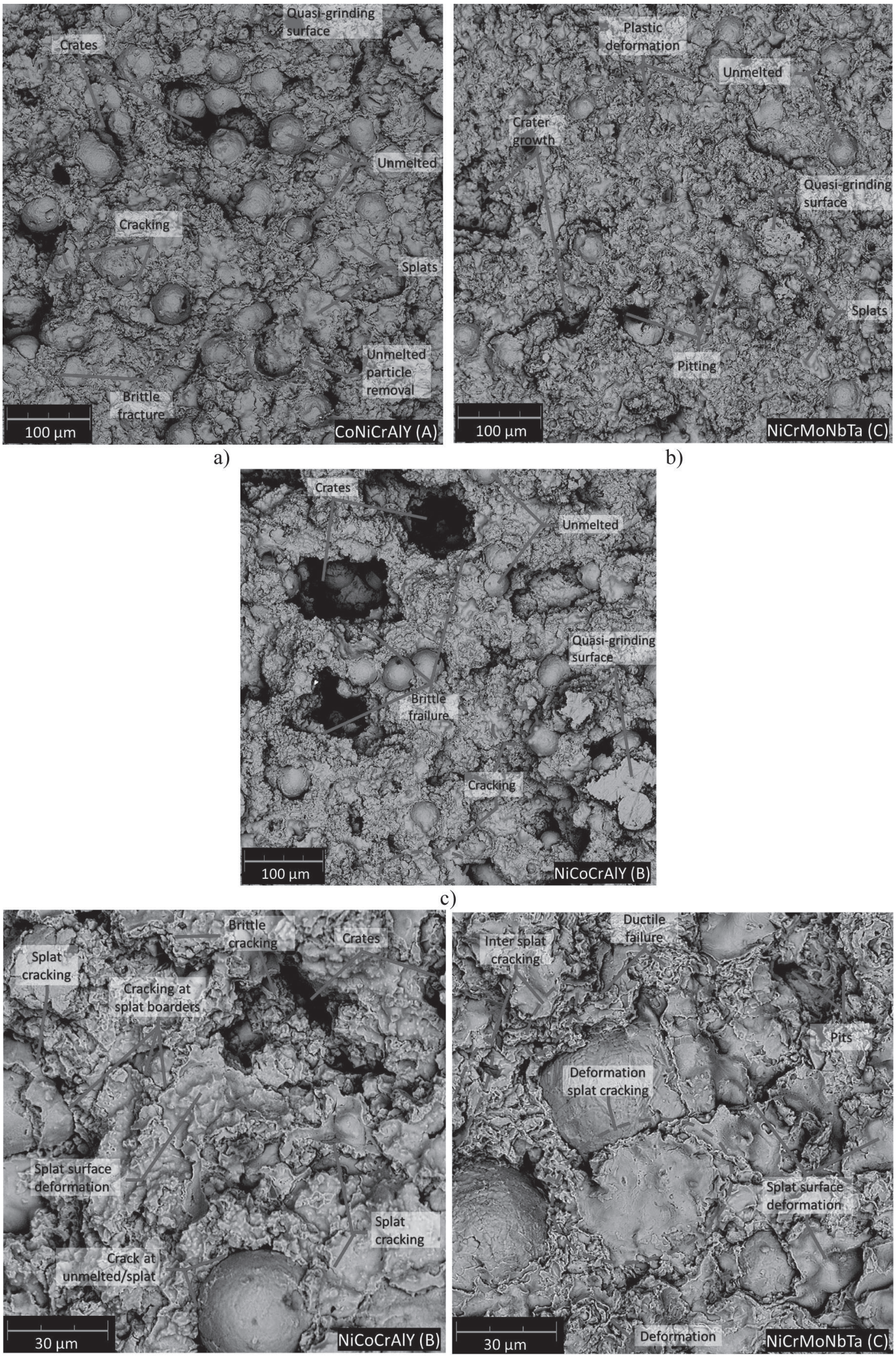

Fig. 5. Cavitation eroded MCrAlYs and NiCrMoNbTa coating: (a–c) comparison of eroded surfaces, x500; (d–e) eroded surfaces, x2000; (f–g) cross-sections, x2000; 3 h of exposure time to cavitation

Rys. 5. Zerodowane powłoki MCrAlYs oraz NiCrMoNbTa (a–c) porównanie zerodowanych powierzchni, x500; (d–e) zerodowane powierzchnie, magn. x2000; (f–g) przekroje poprzeczne, x2000; 3 h ekspozycji na działanie kawitacji

Cavitation erosion phenomenological model of HVOF metallic coatings

The CE phenomenological models of MCrAlY and NiCrMoNbTa are shown in **Fig**. **6**. As presented in **Fig**. **2**, material losses accelerate at the beginning of erosive tests. No CE incubation period characteristic for bulk metallic materials was noted **[L. 30, 31]**. Under the cavitation loads, the grinding coating's surface exhibits detachment of poorly bonded splats and loosely coating material. It contributes to negligible incubation time, which is similar behaviour to the results obtained for other coatings systems such as sprayed plastic coatings **[L. 32]** and APS deposited ceramics **[L. 33]** and composites **[L. 34]**. Besides, microstructural features characteristic for thermal sprayed coatings such as pores, u Nmelted particles, and lamellar splat borders act as erosion centres. Examined coatings differ in microstructure as well as mechanical properties such as hardness and deformability. C coating (NiCrMoNbTa) has better CE behaviour than both A and B (MCrAlYs). CE behaviour analysis conducted using SEM confirms that MCrAlY coatings shows comparable erosion mechanism (**Fig. 5**). Although coating B contains higher amount of aluminium than coating A, which, according to the literature **[L. 27]**, could facilitate the formation of higher content of brittle phases. Besides, in the case of superalloys presence of aluminium favours the formation of strengthening intermetallic phases **[L. 35]**. The softest C-coating presents the most promising CE behaviour compared to tougher ones (A and B coatings), which are discussed in detail in the previous paper **[L. 28]**. The highest material loss was noted for the hardest B coating (393 HV0.1), expressed by the number of arrows in **Fig. 6**. Contrary, coating C (341.6

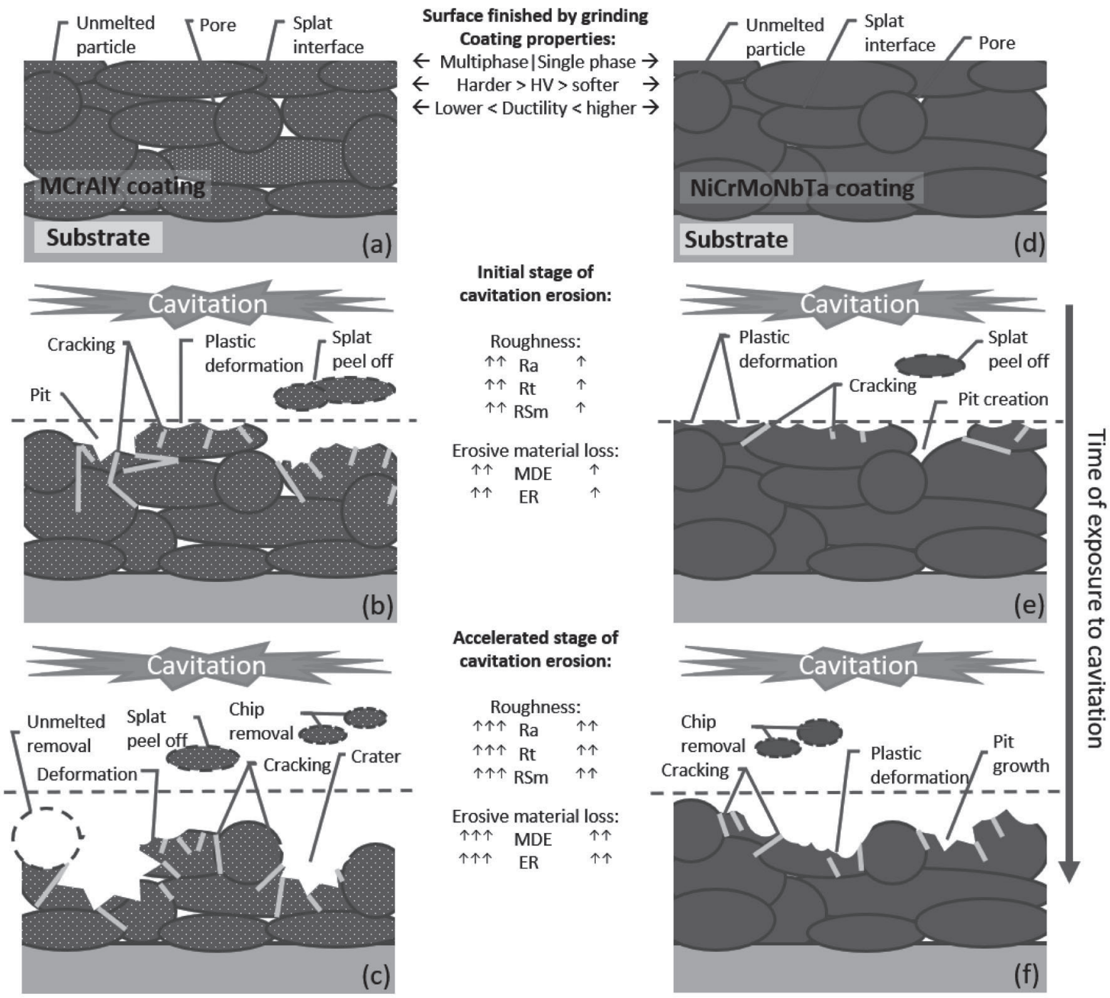

Fig. 6. Cavitation erosion phenomenological model of MCrAlY and NiCrMoNbTa metallic coatings. The number of arrows expresses the increase rate of roughness parameters (Ra, Rz, RSm) and cavitation erosion indicators (MDE and ER)

Rys. 6. Fenomenologiczny model erozji kawitacyjnej metalowych powłok MCrAlY and NiCrMoNbTa. Liczba strzałek wyraża szybkość wzrostu parametrów chropowatości (Ra, Rz, RSm) i wskaźników erozji kawitacyjnej (MDE i ER)

HV0.1) presents minimal depth of erosion (MDE) and erosion rates (ER). Hardness is interpreted as an indicator of coatings deformability. Contrary to brittle behaviour, plasticity usually contributes to the mitigation of the CE rate of metallic materials.

Thus, HVOF metallic coatings ERs differ depending on microstructural features and mechanical properties. Surface roughness is a good indicator of the deformation rate and characterizes the CE damage process well. At the initial stages of erosion, the C coating presents lower MDE and ER than MCrAlYs (**Fig. 2**), which agrees with the previously discussed roughness plots (**Fig. 3**) and conforms to the SEM microscopic observations (**Fig. 5**). Thus, MCrAlYs and NiCrMoNbTa coatings phenomenological models of cavitation erosion differ (**Fig. 6**). Erosion kinetics depends on the higher microstructural uniformity and deformability of C coating than those reported for MCrAlYs. Besides the multiphase structure, the higher hardness (lower ductility) of MCrAlYs facilitates its brittle behaviour under cavitation loads (**Fig. 5d**) which increases the ER of HVOF coatings, **Fig. 2b**. Furthermore, the typical lamellar microstructure of thermally sprayed coatings consisting of splat boarders, u Nmelted powder particles, pores, and different phases borders, which results in the acceleration of deep pits creation and facilitates material removal, especially at initial stages of erosion, see **Fig. 6b** and **e**. Erosive loss progresses by peeling off of splats starting at splat borders, cracking, and the exfoliation of material chips. Spalling of the splats on the surface increases the ER of MCrAlY. It agrees with the findings of Hao et al. **[L. 27]**, who tested the CE resistance of NiCoCrAlYTa coatings in a corrosive enviro Nment. Besides, the rapid mechanical action of cavitation bubbles and collapsing shock waves result in fatigue, cracking, and detachment and plastic deformation, contributing to coating material degradation and loss, shown in **Fig. 5** and **Fig. 6**. Fatigue induced detachment and peeling off are observed in overlapping splats and at splats boarders. Coatings surface degradation relies on cracking, splat fragmentation, and material removal in the form of chips (debris). At further exposure time, pits grow and further create deep craters. On the contrary, in C coating the well-melted splats, denser structure consumes cavitation loads for plastic deformation, which slows down the erosion rate, see **Fig. 5d, e** and **Fig. 6c, f**. Although the erosion mechanism of C is comparable to MCrAlYs (splat detachment, cracking, pit creation), erosive behaviour of C is has a more ductile failure (**Fig. 5d** and **Fig. 6e, f**) than those observed for A and B coatings (**Fig. 5d** and **Fig. 6b, c**). NiCoCrAlY is prone to cracking mainly at splat borders and in severely deformed material (**Fig. 5e**). Contrary to MCrAlY coatings, good ductility of NiCrMoNbTa allows accumulating cavitation loads for plastic deformation and prevents severe material removal.

Profilometric measurements of eroded surfaces MCrAlYs (**Fig. 3**), confirmed that the NiCrMoNbTa coating was characterized by more uniform surface roughness, lesser pitting (lower Ra, Rt and RSm roughness parameters, see **Fig. 3**). This confirms that C coating is prone to plastic deformation, which slowed down the large crater growth and material loss, see **Fig. 5a–c**. Consequently, relatively soft NiCrMoNbTa coating shows an ability to disperse the cavitation loads via plastic deformation (visible in **Fig. 5c)**, while MCrAlY coatings present much more brittle behaviour, resulting in accelerated cracking and material detachment. Finally, at the accelerated stage of erosion, the clusters of deep pits in the surface are visible (**Fig. 5f** and **g**). The MCrAlYs preset deeper erosive craters and high Ra, Rt, and RSm roughness parameters (**Fig. 6c** and **f**).

The MCrAlY coating erosion mechanism has a much more brittle mode than the ductile failure behaviour reported for nickel-based NiCrMoNbTa coating, which presents lower hardness, higher ductility, and higher ductility microstructure uniformity. Microstructure and mechanical properties are crucial factors for increasing the CE resistance of thermally sprayed metallic coatings.

CONCLUSIONS

The analysis of the cavitation erosion (CE) results obtained for MCrAlYs and NiCrMoNbTa metallic coatings deposited on Inconel 617 substrate via the HVOF method allow drawing the following conclusions:

NiCrMoNbTa coating has a higher resistance to cavitation erosion than CoNiCrAlY and NiCoCrAlY coatings. The cumulative mass loss obtained for the MCrAlYs (in the case of NiCoCrAlY coating was over 50% higher) exceeds those reported for NiCrMoNbTa, which also has the lowest maximal erosion rate.

Coating roughness Rz parameter correlates well with mean erosion depth (MDE), while other parameters, Ra, Rt, RSm, provide important information about roughening rate and erosion kinetics. Thus, the roughness rate factor (RR) for the overall characterization of cavitation eroded surfaces morphology and kinetics of the CE process. The RR factor combines the width (RSm), high (Rt) of roughness profile, and mean roughness (Ra) parameters at specific exposure to cavitation time (t).

By combining microstructure, mechanical properties with analysis of surface development done via roughness measurements and SEM observation, the original phenomenological model of cavitation erosion of HVOF metallic coatings was elaborated.

In the case of both MCrAlYs and NiCrMoNbTa coatings, the erosive damage is initiated by removing loosely splats, cracking at the splats border, and peeling off the coating material. However, NiCrMoNbTa, due to higher ductility and microstructure homogeneity, presents lesser surface pitting contrary to the MCrAlYs, which have multiphase microstructure higher hardness and consequently was prone to cracking, resulting in crater formation and severe surface roughening accelerating erosion rate.

The CE mechanism of MCrAlYs was dominated by brittle mode, while NiCrMoNbTa coating mainly has ductile failure behaviour. Moreover, the deformability and dense microstructure of the NiCrMoNbTa coating favours an increase in cavitation erosion resistance.

REFERENCES

1. Łatka L., Niemiec A., Michalak M., Sokołowski P.: Tribological Properties of Al2O3 + TiO2 Coatings Manufactured by Plasma Spraying. Tribologia 2019; 283:19–24. https://doi.org/10.5604/01.3001.0013.1431.
2. Czupryński A.: Flame Spraying of Aluminum Coatings Reinforced with Particles of Carbonaceous Materials as an Alternative for Laser Cladding Technologies. Materials 2019;12:3467. https://doi.org/10.3390/ma12213467.
3. Jonda E., Łatka L.: Comparative Analysis of Mechanical Properties of WC-based Cermet Coatings Sprayed by HVOF onto AZ31 Magnesium Alloy Substrates. Adv Sci Technol Res J 2021; 15:57–64. https://doi.org/10.12913/22998624/135979.
4. Górka J, Czupryński A. The properties and structure of arc sprayed coatings alloy of Fe-Cr-Ti-Si- mN. International Journal of Modern Manufacturing Technologies 2016;8:35–40.
5. Ren Y., Hou G., An Y., Zhao X., Wang Y., Zhou H., et al.: Influence of atomic migration mode at different temperatures on the microstructure, mechanical and cavitation erosion behaviors of Co-based alloy coating. Journal of Alloys and Compounds 2021;866:158989. https://doi.org/10.1016/j.jallcom.2021.158989.
6. Ding X, Ke D, Yuan C, Ding Z, Cheng X.: Microstructure and Cavitation Erosion Resistance of HVOF Deposited WC-Co Coatings with Different Sized WC. Coatings 2018;8:307. https://doi.org/10.3390/coatings8090307.
7. Lavigne S., Pougoum F., Savoie S., Martinu L., Klemberg-Sapieha J.E., Schulz R.: Cavitation erosion behavior of HVOF CaviTec coatings. Wear 2017;386–387:90–8. https://doi.org/10.1016/j.wear.2017.06.003.
8. Szala M., Łatka L., Awtoniuk M., Winnicki M., Michalak M.: Neural Modelling of APS Thermal Spray Process Parameters for Optimizing the Hardness, Porosity and Cavitation Erosion Resistance of Al2O3-13 wt% TiO2 Coatings. Processes 2020;8:1544. https://doi.org/10.3390/pr8121544.

9. Zakrzewska D.E., Krella A.K.: Cavitation Erosion Resistance Influence of Material Properties. Advances in Materials Science 2019;19:18–34. https://doi.org/10.2478/adms-2019-0019.
10. Oksa M., Turunen E., Suhonen T., Varis T., Hannula S.P.: Optimization and characterization of high velocity oxy-fuel sprayed coatings: Techniques, materials, and applications. Coatings 2011;1:17–52. https://doi.org/10.3390/coatings1010017.
11. Tzanakis I., Bolzoni L., Eskin D.G., Hadfield M.: Evaluation of Cavitation Erosion Behavior of Commercial Steel Grades Used in the Design of Fluid Machinery. Metall Mater Trans A 2017;48:2193–206. https://doi.org/10.1007/s11661-017-4004-2.
12. Hattori S., Mikami N.: Cavitation erosion resistance of stellite alloy weld overlays. Wear 2009;267:1954–60. https://doi.org/10.1016/j.wear.2009.05.007.
13. Ronzani A.G., Pukasiewicz A.G.M., da Silva Custodio R.M., de Vasconcelos G., de Oliveira A.C.C.: Cavitation resistance of tungsten carbide applied on AISI 1020 steel by HVOF and remelted with CO_2 laser. J Braz Soc Mech Sci Eng 2020;42:316. https://doi.org/10.1007/s40430-020-02382-7.
14. Varis T., Suhonen T., Laakso J., Jokipii M., Vuoristo P.: Evaluation of Residual Stresses and Their Influence on Cavitation Erosion Resistance of High Kinetic HVOF and HVAF-Sprayed WC-CoCr Coatings. Journal of Thermal Spray Technology 2020;29:1365–81. https://doi.org/10.1007/s11666-020-01037-2.
15. Korobov Yu, Alwan H., Soboleva N., Makarov A., Lezhnin N., Shumyakov V., et al.: Cavitation Resistance of WC-10Co4Cr and WC-20CrC-7Ni HVAF Coatings. J Therm Spray Tech 2021. https://doi.org/10.1007/s11666-021-01242-7.
16. Szala M., Chocyk D., Skic A., Kamiński M., Macek W., Turek M.: Effect of Nitrogen Ion Implantation on the Cavitation Erosion Resistance and Cobalt-Based Solid Solution Phase Transformations of HIPed Stellite 6. Materials 2021;14:2324. https://doi.org/10.3390/ma14092324.
17. Caccese V., Light K.H., Berube K.A.: Cavitation erosion resistance of various material systems. Ships and Offshore Structures 2006;1:309–22. https://doi.org/10.1533/saos.2006.0136.
18. Grist E.: Cavitation And The Centrifugal Pump: A Guide For Pump Users. CRC Press; 1998.
19. Szala M., Walczak M., Hejwowski T.: Factors Influencing Cavitation Erosion of NiCrSiB Hardfacings Deposited by Oxy-Acetylene Powder Welding on Grey Cast Iron. Adv Sci Technol Res J 2021;15:376–86. https://doi.org/10.12913/22998624/143304.
20. Kekes D., Psyllaki P., Vardavoulias M., Vekinis G.: Wear micro-mechanisms of composite WC-Co/Cr-NiCrFeBSiC coatings.Part II: Cavitation erosion. Tribology in Industry 2014;36:375–83.
21. Szala M., Walczak M., Łatka L., Gancarczyk K., Özkan D.: Cavitation Erosion and Sliding Wear of MCrAlY and NiCrMo Coatings Deposited by HVOF Thermal Spraying. Advances in Materials Science 2020;20:26–38. https://doi.org/10.2478/adms-2020-0008.
22. Szala M., Hejwowski T.: Cavitation Erosion Resistance and Wear Mechanism Model of Flame-Sprayed Al2O3-40%TiO2/NiMoAl Cermet Coatings. Coatings 2018;8:254. https://doi.org/10.3390/coatings8070254.
23. Deng W., Hou G., Li S, Han J., Zhao X., Liu X., et al.: A new methodology to prepare ceramic-organic composite coatings with good cavitation erosion resistance. Ultrasonics Sonochemistry 2018;44:115–9. https://doi.org/10.1016/j.ultsonch.2018.02.018.
24. Du J., Zhang J., Zhang C.: Effect of Heat Treatment on the Cavitation Erosion Performance of WC–12Co Coatings. Coatings 2019;9:690. https://doi.org/10.3390/coatings9100690.
25. Ding X., Huang Y., Yuan C., Ding Z.: Deposition and cavitation erosion behavior of multimodal WC-10Co4Cr coatings sprayed by HVOF. Surface and Coatings Technology 2020;392:125757. https://doi.org/10.1016/j.surfcoat.2020.125757.
26. Arora H.S., Rani M., Perumal G., Singh H., Grewal H.S.: Enhanced Cavitation Erosion–Corrosion Resistance of High-Velocity Oxy-Fuel-Sprayed Ni-Cr-Al2O3 Coatings Through Stationary Friction Processing. J Therm Spray Tech 2020;29:1183–94. https://doi.org/10.1007/s11666-020-01050-5.
27. Hao E., An Y., Liu X., Wang Y., Zhou H., Yan F.: Effect of annealing treatment on microstructures, mechanical properties and cavitation erosion performance of high velocity oxy-fuel sprayed NiCoCrAlYTa coating. Journal of Materials Science & Technology 2020;53:19–31. https://doi.org/10.1016/j.jmst.2020.03.030.

28. Szala M., Walczak M., Świetlicki A.: Effect of Microstructure and Hardness on Cavitation Erosion and Dry Sliding Wear of HVOF Deposited CoNiCrAlY, NiCoCrAlY and NiCrMoNbTa Coatings. Materials 2022;15:93. https://doi.org/10.3390/ma15010093.
29. ASTM G32-16 Standard Test Method for Cavitation Erosion Using Vibratory Apparatus 2016. https://doi.org/10.1520/G0032-16.
30. Fatyukhin D.S., Nigmetzyanov R.I., Prikhodko V.M., Sukhov A.V., Sundukov S.K.: A Comparison of the Effects of Ultrasonic Cavitation on the Surfaces of 45 and 40Kh Steels. Metals 2022;12:138. https://doi.org/10.3390/met12010138.
31. Rostova H., Voyevodin V., Vasilenko R., Kolodiy I., Kovalenko V., Marinin V., et al.: Cavitation wear of Eurofer 97, Cr18Ni10Ti and 42H NM alloys. Acta Polytechnica 2021;61:762–7. https://doi.org/10.14311/AP.2021.61.0762.
32. Szala M., Świetlicki A., Sofińska-Chmiel W.: Cavitation erosion of electrostatic spray polyester coatings with different surface finish. Bulletin of the Polish Academy of Sciences Technical Sciences 2021;69:e137519. https://doi.org/10.24425/bpasts.2021.137519.
33. Łatka L., Michalak M., Szala M., Walczak M., Sokołowski P., Ambroziak A.: Influence of 13 wt% TiO2 content in alumina-titania powders on microstructure, sliding wear and cavitation erosion resistance of APS sprayed coatings. Surface and Coatings Technology 2021;410:126979. https://doi.org/10.1016/j.surfcoat.2021.126979.
34. Szala M., Dudek A., Maruszczyk A., Walczak M., Chmiel J., Kowal M.: Effect of atmospheric plasma sprayed TiO2-10% NiAl cermet coating thickness on cavitation erosion, sliding and abrasive wear resistance. Acta Phys Pol A 2019;136:335–41. https://doi.org/10.12693/APhysPolA.136.335.
35. Derelizade K., Rincon A., Venturi F., Wellman R.G., Kholobysov A., Hussain T.: High temperature (900°C) sliding wear of CrNiAlCY coatings deposited by high velocity oxy fuel thermal spray. Surface and Coatings Technology 2022:128063. https://doi.org/10.1016/j.surfcoat.2021.128063.